

A Tris(triphenylphosphine)ruthenium(II) Complex as a UV Photoinitiator for Free-Radical Polymerization and *in Situ* Silver Nanoparticle Formation in Cationic Films

Davy-Louis Versace,^{†,*} Javier Cerezo Bastida,[‡] Cédric Lorenzini,[†] Christine Cachet-Vivier,[†] Estelle Renard,[†] Valérie Langlois,[†] Jean-Pierre Malval,[§] Jean-Pierre Fouassier,^{⊥,#} and Jacques Lalevée^{§,*}

[†]Institut de Chimie et des Matériaux Paris-Est, UMR 7182, Université Paris-Est Créteil Val de Marne (UPEC), 2-8 rue Henri Dunant, 94320 Thiais, France

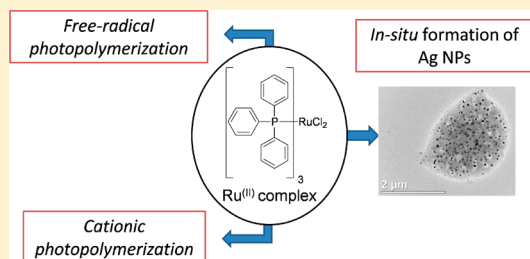
[‡]Departamento de Química Física, Universidad de Murcia, 30100 Murcia, Spain

[§]Institut de Science des Matériaux de Mulhouse, UMR CNRS-UHA 7361, 15 rue Starcky - 68057 Mulhouse, France

[⊥]ENSCMu-UHA, 3 rue Alfred Werner, 68093 Mulhouse Cedex, France

Supporting Information

ABSTRACT: The characterization and the photochemical investigation of a Ru^{II} complex (Ru(PPh₃)₃Cl₂) having phosphine ligands are reported. DFT calculations and ESR spin trapping experiments revealed for the first time that the photodecomposition of the complex is governed by a homolytic cleavage of the P–(C₆H₅) bond generating phenyl radicals Ph• which are able to initiate the free radical polymerization of acrylate monomers. The addition of a H-donor HD plays a key role in the cationic photopolymerization of epoxides: (i) the reaction efficiency is enhanced using [Ru(PPh₃)₃Cl₂]/HD and (ii) the *in situ* formation of Ag nanoparticles is observed in the presence of Ru(PPh₃)₃Cl₂/HD/AgSbF₆ according to the following reactions: Ph•/DH hydrogen abstraction yielding a D• radical and oxidation of D• by the silver salt.



INTRODUCTION

In the past years, there has been a growing interest in the use of ruthenium Ru^{II} complexes containing phosphines in both organic transformations and polymer synthesis. Such complexes are of considerable interest as they find applications in classical catalytic processes, e.g., aerobic oxidation,¹ hydrogenation,² isomerization,³ reductive elimination⁴ or decarbonylation,⁵ and metathesis activity;⁶ more recently, they have been applied as catalysts in metal-catalyzed living radical polymerization reactions.⁷ They are active toward a large variety of monomers, their versatility stemming from the flexible modification of their properties through the introduction of various ligands. Moreover, they present a high stability in alcoholic solvents⁸ due to the low oxophilicity of the ruthenium atom, thereby allowing the synthesis of polymer architectures including functionalized random, block and star polymers in polar solvents (see for example in ref 9 their use in the living polymerization of MMA and HEMA in conjunction with a series of bulky fluoroalcohols at 0 °C or the synthesis of syndiotactic-*b*-atactic poly(HEMA) by changing both the nature of the solvent and the temperature). The widely used complex RuCl₂(PPh₃)₃ suffers, however, from two severe limitations: a relatively high catalyst concentration is needed and rather harsh reaction conditions (temperature between 100 and 120 °C) are often used;¹⁰ moreover, the addition of cocatalyst (like a aluminum-derived compound)¹¹ is often

necessary for getting a faster and a better controlled polymerization.

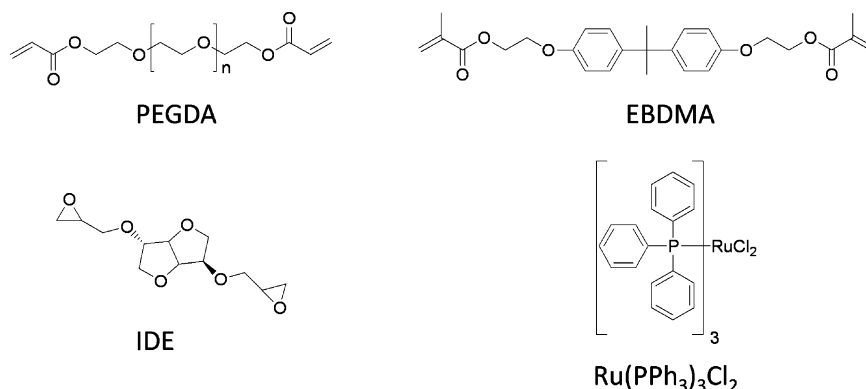
Some efforts have been devoted so far to design efficient ruthenium catalysts which can be activated under light activation. Indeed, compared to a thermal activation, a photochemical route provides numerous advantages,¹² e.g., the use of mild experimental conditions. For example, the photopolymerization of acrylamide using Ru^{II}-catalysts has been described in the 80s (see review in ref 13) and the photoactivated metathesis polymerizations where Ru^{II}-based complexes are used as precatalysts have been reported.¹⁴ More recently, a new photoredox catalysis approach involving ruthenium (or iridium, zinc) complexes and various additives and working through oxidation or reduction cycles was proposed to initiate the free radical polymerization FRP of acrylates, the cationic polymerization CP of epoxides or the free radical promoted cationic photopolymerization FRPCP of *N*-vinylcarbazole, epoxides or renewable cationic monomers under soft irradiation conditions in the visible wavelength range.¹⁵ In the same way, photoactivated catalytic systems (based on cyclometalated Ru^{II} complexes containing strongly coordinating bidentate ligands) in conjunction with traditional

Received: September 25, 2013

Revised: November 7, 2013

Published: November 19, 2013

Scheme 1. Structure of the Monomers and Photoinitiator Used in This Study



alkyl bromides have been also developed for the free radical polymerization of hydrophobic monomers,¹⁶ i.e., methyl methacrylate, styrene, and *n*-butyl acrylate.

In the present paper, we will explore the *in situ* formation of silver nanoparticles in a curable neat epoxide matrix using a ruthenium complex as a photoinitiator (PI) incorporated into a suitable photoinitiating system (PIS). This has never been checked although a lot of organic PI and PIS (based on ketones, e.g., benzoin ethers, acyl germanes, benzophenones, or thioxanthenes; hydrocarbons, e.g., pyrene or anthracene derivatives; and dyes, e.g., eosin) have been tested for the production of metal NPs (see, e.g., in ref 17). The well-known compound $RuCl_2(PPh_3)_3$ is selected here as an example: compared to other Ru^{II} based complexes, it should work as a one-component PI, a cleavage of the ligands being expected. TD-DFT calculations, UV spectroscopy, steady state photolysis, electron spin resonance spin-trapping experiments, TEM measurements and EDX spectroscopy will allow a complete description of the absorption properties of $RuCl_2(PPh_3)_3$, the generation of radicals, the mechanisms involved in the initiation step of the FRP of (meth)acrylates (PEGDA and EBDMA) and the CP/FRPCP of a renewable diepoxide monomer (diallyl isosorbide ether, IDE) as well as the formation of Ag NPs in solution and in film.

EXPERIMENTAL SECTION

Chemical Compounds. All reagents and solvents were purchased from Aldrich and used as received without any further purification. ¹H and ¹³C NMR spectra were recorded at room temperature in 5 mm o.d tubes on a Bruker Avance 400 spectrometer: ¹H (400 MHz) and ¹³C (100 MHz). The ¹H chemical shifts were referenced to the solvent peak CDCl₃ (7.26 ppm), and the ¹³C chemical shifts were referenced to the solvent peak CDCl₃ (77.0 ppm). Isosorbide diglycidyl ether (IDE) were prepared following the literature procedure and obtained in similar yield. Tris(triphenylphosphine)ruthenium(II) dichloride (97%, $Ru(PPh_3)_3Cl_2$) and silver hexafluoroantimonate (98%, $AgSbF_6$) were obtained from Sigma-Aldrich. Poly(ethylene glycol) (400) diacrylate (PEGDA, SR 344) and ethoxylated bisphenol A dimethacrylate (EBDMA, SR348) were kindly provided by Sartomer, Arkema group. Isosorbide diglycidyl ether was selected as a representative epoxy monomer (Scheme 1).

Synthesis of Isosorbide Diglycidyl Ether (IDE). Diallyl isosorbide ether was prepared by the Williamson reaction. Isosorbide (3 g, 20.4 mmol) was dissolved in a 50% aqueous NaOH (6g, 107.2 mmol) solution. Allyl bromide (10 mL, 115.7 mmol) was used as an alkylating agent in the presence of 4.6% of tetrabutylammonium bromide (TBAB, 300 mg, 0.94 mmol) with respect to isosorbide. The reaction was stopped after 4 h of heating at 65 °C and the mixture was extracted with methylene chloride. Freshly prepared diallyl isosorbide

(3 g, 13.4 mmol) was then added slowly to a solution of *m*-chloroperbenzoic acid (7 g, 40.6 mmol) in 12 mL of methylene chloride. The reaction was stirred at a temperature of 20 °C for 72 h. The solution was then filtrated and washed with a solution of 10% sodium bisulfate followed by saturated sodium bicarbonate and distilled water. The organic layer was then dried over magnesium sulfate. The yield of the reaction is 60%. ¹H and ¹³C NMR spectra of the synthesized epoxy monomer were displayed in the Supporting Information part (Figures S1 and S2).

Photopolymerization Procedures. For the free radical photopolymerization, $Ru(PPh_3)_3Cl_2$ (1 wt % with respect to the acrylate monomer) was dissolved into acrylate monomer formulation (PEGDA or EBDMA, 1 g) containing 1 mL of THF or ACN. For free-radical promoted cationic polymerization of the epoxy monomer (IDE, 1 g), four photoinitiating systems have been tested: (1) $Ru(PPh_3)_3Cl_2$ (1 wt % with respect to IDE)/ACN (0.5 mL), (2) $Ru(PPh_3)_3Cl_2/AgSbF_6$ (1/3 wt % with respect to IDE)/ACN (0.5 mL), (3) $Ru(PPh_3)_3Cl_2$ (1 wt % with respect to IDE)/THF (0.5 mL), and (4) $Ru(PPh_3)_3Cl_2/AgSbF_6$ (1/3 wt % with respect to IDE)/THF (0.5 mL). Kinetics of photopolymerization were followed by real time Fourier transform infrared spectroscopy (RT-FTIR) using a Thermo-Nicolet 6700 instrument. The liquid samples were applied to a BaF₂ chips by means of calibrated wire-wound applicator. The thickness of the UV-curable film was evaluated at 4 μm. The RT-FTIR analyses were carried out under laminated conditions: a polypropylene film was laid on the top of the photosensitive layer to prevent oxygen diffusion. Samples were irradiated at room temperature, by means of a Lightningcure LC8 (L8251) from Hamamatsu, equipped with a mercury–xenon lamp (200 W) coupled with a flexible light guide. The end of the guide was placed at a distance of 6 cm. The maximum UV light intensity at the sample position was evaluated to be 150 mW/cm². The photopolymerization was monitored by the disappearance of the carbon double bonds of the acrylate derivative monomers at 1636 cm⁻¹ (for poly(ethylene glycol) (400) diacrylate and ethoxylated bisphenol A dimethacrylate) and the epoxide group¹⁸ at 1247 cm⁻¹ (for isosorbide diglycidyl ether).

UV–Vis Spectroscopy. UV spectra were recorded on a Varian spectrophotometer (Cary 50 bio).

ESR Experiments. ESR spin-trapping experiments were carried out using an X-Band EMX spectrometer (Bruker Biospin). The radicals were generated at room temperature using polychromatic light irradiation (Xe–Hg lamp; Hamamatsu, L8252, 150 W) and trapped by phenyl-*N-tert*-butylnitron (PBN) according to a procedure described in detail in ref 19. The ESR spectra simulations were generated using the PEST WINSIM program. All of the samples were prepared in a 6 mm quartz cylindrical tube and dissolved in *tert*-butylbenzene as an inert solvent.

Laser Flash Photolysis. Nanosecond laser flash photolysis (LFP) experiments were carried out using a Q-switched nanosecond Nd/YAG laser at $\lambda_{exc} = 355$ nm (9 ns pulses; energy reduced down to 10 mJ; minilite Continuum) and the analyzing system consisted of a

pulsed xenon lamp, a monochromator, a fast photomultiplier and a transient digitizer²⁰ (Luzchem LFP 212).

Redox Potentials. The electrochemical studies were carried out in a three-electrode cell using an AUTOLAB PT30 potentiostat (METROHM). The working electrode was a platinum disk (2 mm diameter) which was carefully polished with an abrasive paper before measurements. The counter-electrode was a gold wire and the reference one a saturated calomel electrode (SCE). Acetonitrile was distilled and used as solvent, and tetrabutylammonium tetrafluoroborate (NBu_4BF_4) as supporting electrolyte with a concentration of 0.1 mol. L^{-1} . Ruthenium complex, silver salt or triphenylphosphine were added to this electrolytic solution for obtaining a 10^{-2} mol L^{-1} concentration. NBu_4BF_4 was dried at 100 °C before use. All the solutions were deoxygenated by bubbling N_2 gas.

Transmission Electron Microscopy. observations were conducted on a Tecnai F20 ST microscope (field-emission gun operated at 3.8 kV extraction voltage) operating at an acceleration voltage of 200 kV and equipped with an X-ray energy-dispersive spectrometer (XEDS from Oxford Instruments) for chemical analysis. The samples were prepared as follows: a 15 μL drop of acetonitrile nanoparticle suspension was deposited on a carbon-coated 400 mesh copper grid.

DFT Calculations. The structure of tris(triphenylphosphine)-ruthenium was initially modeled using the experimental X-ray structural parameters given by LaPlaca et al.²¹ and subsequently optimized by DFT methods, using the B3LYP functional along with the Stuttgart–Dresden basis set and pseudopotentials for ruthenium, additionally including an extra *f* polarization function with a coefficient of 0.96, the Ahlrichs triple- ξ , pVTZ, for carbon, chlorine, and phosphorus, and Ahlrichs double- ξ , pVDZ, for hydrogen. Such combination of basis set and functional has been previously proven to be useful in the calculation of other ruthenium complexes. The effect of the solvent, i.e., acetonitrile, was included through the conductor-like PCM algorithm (CPCM). A time-dependent (TD) calculation was performed on the optimized structure at TD-B3LYP level using the same basis set as for the optimization and the CPCM algorithm to account for solvent (acetonitrile) effects. The most relevant transitions were analyzed by computing the natural transition orbitals (NTO), which offers a compact orbital representation for electronic transitions and reveals very useful to characterize the transitions when more than one monoexcitation is relevant for the transition using canonical orbitals, as was actually the case.

RESULTS AND DISCUSSION

1. Absorption Properties of $[\text{Ru}(\text{PPh}_3)_3\text{Cl}_2]$ Complex.

The fully optimized geometry of the complex ruthenium is displayed in Figure 1A. As expected, the metal complex exhibits a distorted square pyramidal geometry in agreement with the crystallographic structure.²¹ Although the global trends are well reproduced, this calculated DFT structure displays slightly larger bond lengths as compared with those reported in the X-ray structure (~ 0.1 Å for Ru–P and Ru–Cl). For instance, the apical Ru–P bond was found to be around 0.2 Å shorter than the basal Ru–P distances, while the two Ru–Cl bonds are of similar length and shorter than the basal Ru–P. The distorted geometry of a pentacoordinated complex can be further characterized through the τ parameter which is defined as the difference between the two largest X–Metal–Y angle in degrees divided by 60 and whose value ranges from 1 for a trigonal pyramidal (TBP) to 0 for a square pyramidal geometry. The crystallographic and DFT computed values of τ are 0.01 and 0.02, respectively, with P–Ru–P and Cl–Ru–Cl angles also similar between X-ray and DFT, being 156.4 and 157.2 (X-ray), and 157.4 and 158.8 (DFT). The ability of the DFT methods to reproduce the experimental geometry was nevertheless observed and, interestingly, the DFT level leads to a structure closer to the crystallographic one, further validating our procedure.

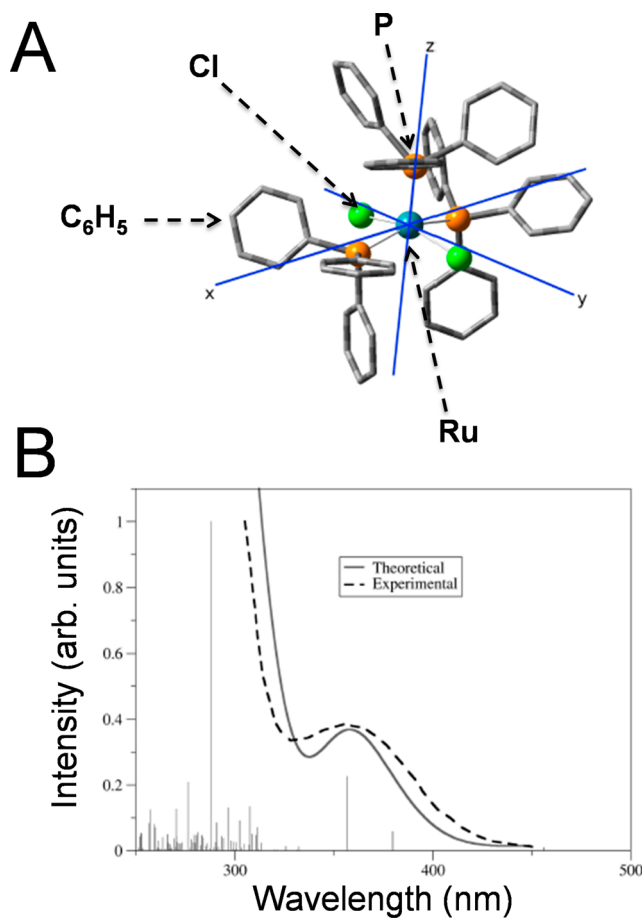


Figure 1. (A) Representation of $\text{Ru}(\text{PPh}_3)_3\text{Cl}_2$ optimized at B3LYP/LANL2DZ level and (B) comparison of the experimental (dashed line) and the theoretical (solid line) spectra of tris(triphenylphosphine)ruthenium dichloride ($\text{Ru}(\text{PPh}_3)_3\text{Cl}_2$). The theoretical spectrum of $\text{Ru}(\text{PPh}_3)_3\text{Cl}_2$, optimized at B3LYP/LANL2DZ level and computed at TD-B3LYP/LANL2DZ levels, includes the solvent effect (acetonitrile).

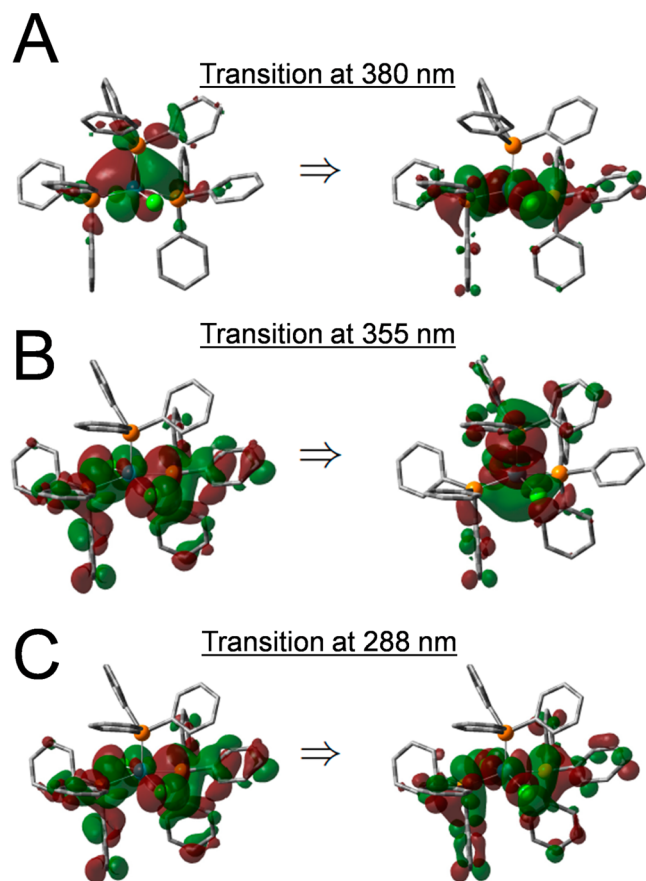
Regarding the spectroscopic properties, the UV–visible absorption spectrum obtained in acetonitrile shows weakly intense bands at around 355 and 385 nm and a more intense one below 300 nm (Figure 1B). The vertical transitions calculated by the TD-DFT method nicely match the experimental ones and, therefore, allow a confident assignment of these spectroscopic bands as shown in Figure 1B. Natural transition orbitals²² (NTOs) offer the most compact view of an excited state as a single orbital transition from the ground state, and therefore have been computed to facilitate the spectroscopic assignment using the usual descriptions based on orbital transitions. Note that, in the nomenclature of NTOs, the transition is as follows: hole \rightarrow particle. For instance, the contribution of each fragment can be measured through the contribution of the corresponding atomic orbitals to the NTO. By computing the contributions at the hole and at the particle NTO, one has an idea about how the electronic distribution can be changed upon the transition. The contributions of each relevant transition are shown in Table 1. This information, together with the representation of the corresponding NTO (Figure 2), can be used to identify the nature of each state.

According to Table 1 and Figure 2, the assignment of the three main transitions can be ascribed as follow:

Table 1. Contribution (%) of the Atomic Orbitals for each Fragment to Hole and Particle NTOs^a

fragment	transition at 380 nm		transition at 357 nm		transition at 288 nm	
	hole	particle	hole	particle	hole	particle
metal Ru	14.2	15.7	4.4	12.5	3.8	13.9
chlorine 1	0.3	5.6	5.3	3.2	4.9	3.9
chlorine 2	0.6	5.3	4.0	3.7	4	3.7
phosphine 1	34.0	13.0	10.0	35.9	10.5	12.7
phosphine 2	24.2	29.6	38.8	22.5	39.1	32.8
phosphine 3	26.7	30.8	37.4	22.3	37.7	33.0

^a“Phosphine 1” is ascribed to the apical one.

**Figure 2.** Natural transition orbitals computed at TD-DFT level for the transitions at (A) 380, (B) 355, and (C) 288 nm including the solvent effect (acetonitrile).

- Transition at 380 nm: In this case, Table 1 indicates a significant charge transfer from the apical phosphine toward basal ones, thus leading a transition with a remarkable Interligand charge transfer (ILCT character).
- Transition at 355 nm: It can be considered as an interligand charge transfer, as the electronic density over the basal ligands in the initial orbital is transferred to the apical ligand in the final one. Figure 2 indicates that this charge transfer arises along the transition from d_{xz} to $d_{x^2-y^2}$ in the metal.
- Transition at 288 nm: This transition does not involve a significant charge displacement as it remains in the base of the pyramid, but a change of the metal orbital is

observed, i.e., a $d \rightarrow d$ transition from the d_{xz} orbital to the d_{z^2} orbital.

It is worth noticing that a weak spectroscopic band at around 615 nm appears and is associated with an electronic transition that displays an important metal to ligand charge transfer (MLCT) character. Concretely, the transition goes from a metal-centered orbital, d_{xz} , to a hybrid molecular orbital mixing the d_{z^2} orbital on the metal with an antibonding orbital on the apical triphenylphosphine ligand (Figure S3, see Supporting Information).

2. Photochemical Properties of $[\text{Ru}(\text{PPh}_3)_3\text{Cl}_2]$ Complex. The steady state photolysis of the $\text{Ru}(\text{PPh}_3)_3\text{Cl}_2$ complex was carried out in acetonitrile (Figure 3). A very fast photobleaching occurs as revealed by the decrease of the absorption band at 355 nm.

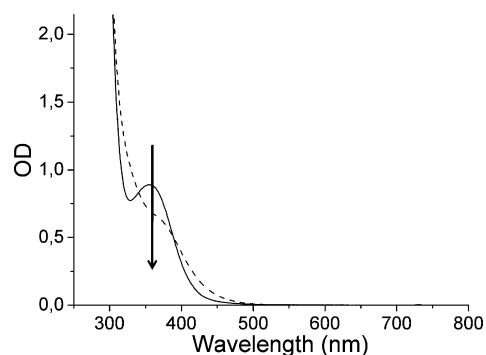
**Figure 3.** Photolysis of $\text{Ru}(\text{PPh}_3)_3\text{Cl}_2$ in acetonitrile. $[\text{Ru}(\text{PPh}_3)_3\text{Cl}_2] = 1.13 \times 10^{-3} \text{ mol L}^{-1}$. Irradiation = Hg–Xe lamp; $I_0 = 150 \text{ mW cm}^{-2}$. Key: (—) before irradiation, (---) after 300 s of irradiation.

Figure 4 displays the experimental and calculated ESR-ST spectra recorded after the UV irradiation (200–400 nm) of $\text{Ru}(\text{PPh}_3)_3\text{Cl}_2$ under argon saturated *tert*-butylbenzene (Figure 4A) or toluene (Figure 4B). The presence of a phenyl radical ($\text{C}_6\text{H}_5^\bullet$) resulting from the homolytic P–(C_6H_5) single bond photocleavage (Scheme 2) is clearly supported (Figure 4A; hfc of the PBN radical adduct: $a_{\text{N}} = 14.1\text{G}$ and $a_{\text{H}} = 2.1\text{G}$ in agreement with known values²³). The phenyl reacts with toluene and yields a benzyl radical: both kinds of PBN radical adducts are observed in Figure 4B: (i) $a_{\text{N}} = 13.6\text{G}$ and $a_{\text{H}} = 2\text{G}$ for the phenyl and (ii) $a_{\text{N}} = 14.3\text{G}$ and $a_{\text{H}} = 2.9\text{G}$ for the benzyl. Surprisingly, the expected phosphorus-centered radical $\text{Ru}(\text{PPh}_3)_2(\bullet\text{PPh}_2)\text{Cl}_2$ (Scheme 2) is not trapped by PBN. This could be explained by (i) the short lifetime of the phosphorus-centered radical²⁴ (<100 ns) or/and (ii) the unfavorable addition of this crowded radical to PBN (indeed, the unpaired electron in the SOMO of $\text{Ru}(\text{PPh}_3)_2(\bullet\text{PPh}_2)\text{Cl}_2$ is mainly delocalized over a π orbital of the PPh_2 ligand and the empty d_{z^2} orbital of the ruthenium complex as shown in Figure 5). No transient absorption and bleaching are observed in laser flash photolysis experiments suggesting a relatively low dissociation quantum yield.

3. Redox Properties of $[\text{Ru}(\text{PPh}_3)_3\text{Cl}_2]$ Complex. The comparison of the cyclic voltammograms of $\text{Ru}(\text{PPh}_3)_3\text{Cl}_2$ and a free triphenylphosphine (Figure 6) reveals that the anodic and cathodic peaks respectively located at 1.48 and 1.25 V/SCE are specific of the Ru^{II} complex. The cyclic voltammogram of Ph_3P in ACN shows three successive oxidation waves whose identification has been previously reported.²⁵ The first oxidation wave ($E \sim 0.50 \text{ V vs SCE}$) corresponds to the

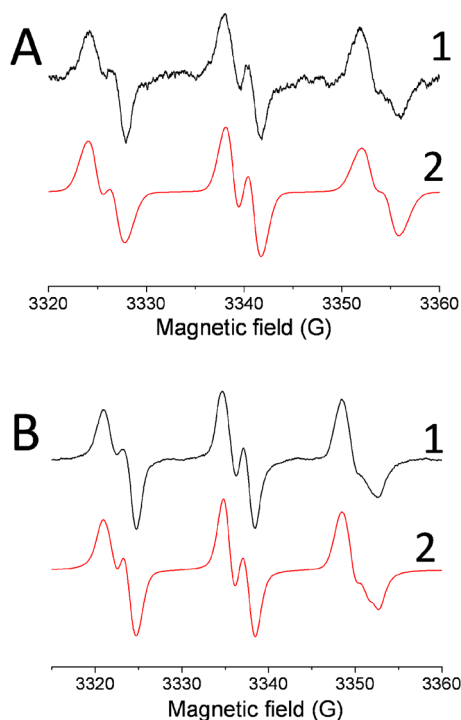
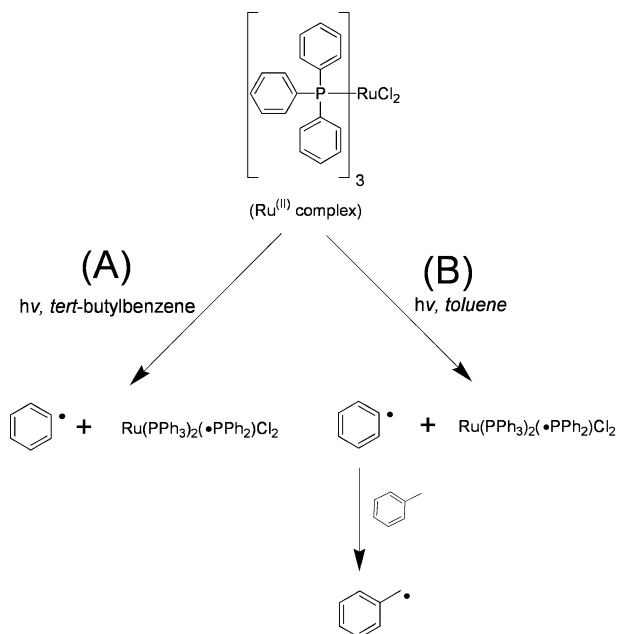


Figure 4. ESR spin trapping experimental (1) and simulated (2) spectra obtained during irradiation of $\text{Ru}(\text{PPh}_3)_3\text{Cl}_2$ under argon (A) in *tert*-butylbenzene and (B) in *tert*-butylbenzene/toluene. Xenon–mercury lamp exposure. PBN: 0.05 M.

Scheme 2. Mechanistic approach to $[\text{Ru}(\text{PPh}_3)_3\text{Cl}_2]$ Complex Photolysis under Argon Saturated Atmosphere in (A) *tert*-Butylbenzene and (B) Toluene^a



^aThe UV light intensity is 180 mW/cm². Radicals are trapped by PBN.

oxidation of triphenylphosphine to triphenylphosphonium radical whereas the other waves correspond to the oxidation of secondary products stemming from a reaction between this generated radical cation with residual water in the solvent. As proposed by Ohmori et al,^{25b} a very fast redox reaction occurs between $^+\text{PPh}_3$ with residual water yielding triphenylphos-

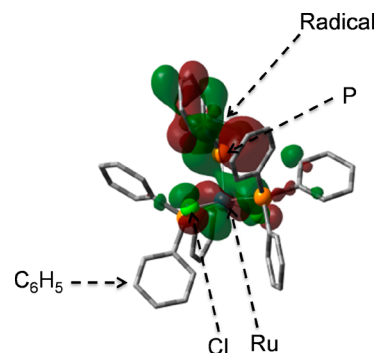


Figure 5. SOMO of the radical ruthenium complex ($\text{Ru}(\text{PPh}_3)_2(\bullet\text{PPh}_2)\text{Cl}_2$) after the homolytic cleavage of one of the apical P–Ph bonds, computed at DFT level.

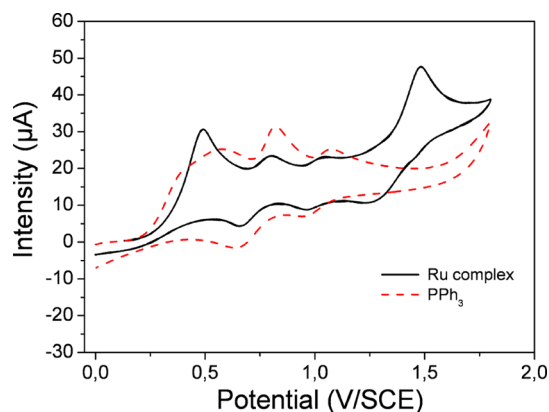


Figure 6. Cyclic voltammograms of $[\text{Ru}(\text{PPh}_3)_3\text{Cl}_2]$ complex (solid line) and triphenylphosphine (dash line) in acetonitrile.

phine oxide (Ph_3PO) and a proton which sequentially reacts with a Ph_3P molecule to generate Ph_3PH^+ . It should be noted that these multiple oxidation waves are also observed for the ruthenium complex and do not affect the positions of anodic and cathodic peaks of the metal.

4. Photoinduced Generation of Silver Nanoparticles.

Figure 7 shows the typical evolution of the absorption spectrum of $\text{Ru}(\text{PPh}_3)_3\text{Cl}_2$ mixed with an excess of silver salt (AgSbF_6) in oxygen-free acetonitrile under UV irradiation. The rapid increase (within ~ 15 s) of a large band with a maximum located at 450 nm can be safely assigned to the known²⁶ silver surface plasmon band. The Ag formation can be explained as resulting from two reactions. First, an electron transfer between the excited state of $\text{Ru}(\text{PPh}_3)_3\text{Cl}_2$ and AgSbF_6 is favorable. Indeed, according to the Rehm–Weller equation, the ΔG for this electron transfer is negative ($\Delta G = -1.7$ eV using $E_{\text{Red}}(\text{AgSbF}_6) = +0.21$ V/SCE and $E_{\text{Ox}}(\text{Ru}(\text{PPh}_3)_3\text{Cl}_2) = +0.5$ V/SCE; the triplet state energy level of $\text{Ru}(\text{PPh}_3)_3\text{Cl}_2$ is not known but is probably close to 2 eV as evaluated from the red-shifted absorption (see above) at 615 nm). Second, the phosphinyl radical generated during the photolysis of $\text{Ru}(\text{PPh}_3)_3\text{Cl}_2$ (Scheme 2) is oxidized by AgSbF_6 : this process is similar to the reduction of an onium salt by a phosphinoyl radical as described in.²⁷ The addition of a H-donor solvent such as THF (Figures 7C and 7D) accelerates the formation of the silver nanoparticles²⁸ according to reactions 1 and 2. EDX and TEM experiments confirm the formation of Ag NPs. The EDX spectroscopy carried out on the $\text{Ru}(\text{PPh}_3)_3\text{Cl}_2/\text{AgSbF}_6$ acetonitrile solution (Figure 8) reveals an intense silver peak at

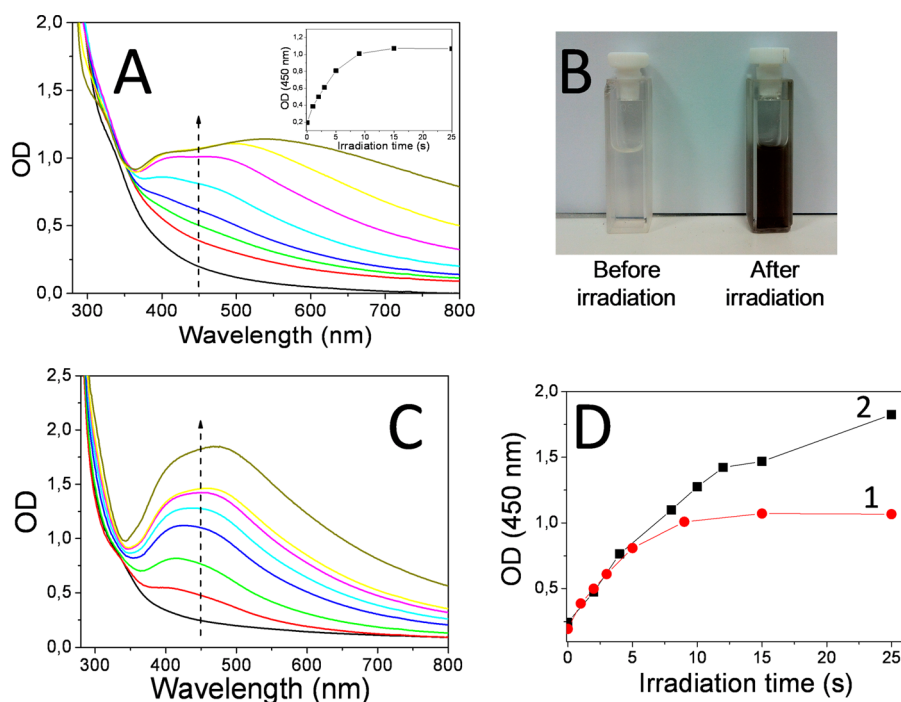


Figure 7. (A) Evolution of the absorption spectra during the irradiation of Ru(PPh₃)₃Cl₂ (3×10^{-4} mol L⁻¹)/AgSbF₆ (1.3×10^{-3} mol L⁻¹) in acetonitrile. Inset: evolution of the absorbance change at 450 nm with the irradiation time. (B) Sample before and after 15 s of irradiation. (C) Evolution of the absorption spectra during the irradiation of Ru(PPh₃)₃Cl₂ (3×10^{-4} mol L⁻¹)/AgSbF₆ (1.3×10^{-3} mol L⁻¹)/THF (2 mL). (D) Evolution of the Ag NPs formation (absorbance at 450 nm) in the absence (1) and presence of THF (2). All the solutions are degassed with argon prior to irradiation. Hg–Xe lamp; $I_0 = 150$ mW cm⁻².

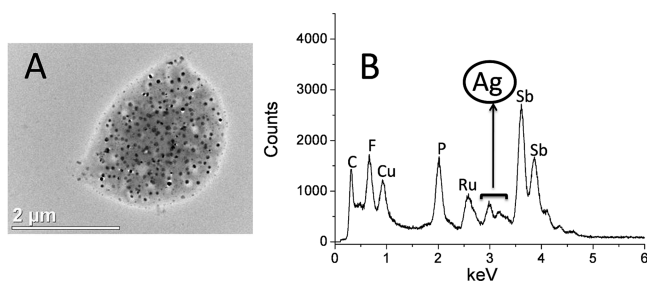
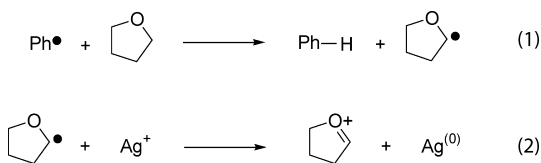


Figure 8. (A) TEM image of the photoinduced silver nanoparticles solution and (B) EDX spectra acquired in STEM. Xenon–mercury lamp exposure (15 s, argon atmosphere).

3 eV, thus indicating the presence of substantial amounts of Ag⁽⁰⁾ in the analyzed area. The TEM image of the photoinduced silver nanoparticles solution is also shown in Figure 8.

5. Photopolymerization of Acrylate Matrixes with [Ru(PPh₃)₃Cl₂] Complex. The photopolymerization profiles of a diacrylate (PEGDA) and a dimethacrylate monomers (EBDMA) in laminate upon UV light exposure in the presence of Ru(PPh₃)₃Cl₂ are displayed in Figure 9 (to increase the solubility of the Ru complex, a small amount (1 mL) of THF or ACN was introduced). Final conversions are almost 100% after 50 s of irradiation for PEGDA but only 70% after 300s for EBDMA. The phenyl radicals are obviously the initiating

species according to the ESR spin-trapping results and the very high k_i (of phenyl radicals) to acrylates.¹² It should be pointed out that during the free-radical photopolymerization of the acrylate monomers, an induction period is observed. Indeed, during the photoinitiating process, the remaining oxygen molecules of the photopolymerized solution react with radical species to generate inert peroxy radicals ROO[•] that are not reactive toward the acrylate double bonds and cannot initiate any polymerization reaction¹² (induction period). When all the oxygen molecules are consumed, the photopolymerization can start.

6. Photopolymerization of Epoxy Matrix with [Ru(PPh₃)₃Cl₂] complex/AgSbF₆. The irradiation of a diepoxide in laminate using Ru(PPh₃)₃Cl₂ (1 wt %) in the presence of ACN (0.5 mL) or THF (0.5 mL) does not lead to any efficient polymerization (Figure 10, parts A-1 and B-1; final conversion, 10% after 300 s of irradiation). The addition of AgSbF₆ (3 wt %) to Ru(PPh₃)₃Cl₂/ACN (Figure 10A-2) has no influence on the final conversion. Interestingly, the use of Ru(PPh₃)₃Cl₂/AgSbF₆/THF (Figure 10B-2) leads to a significant improvement of the cationic polymerization (the final conversion increases from 10% to 50% and exhibits a brown coloration thereby confirming the presence of Ag NPs). This suggests that the *in situ* reduction of the silver salt to Ag mainly occurs according to eq1 and eq2; the main initiating cationic species is the THF cation.

CONCLUSION

In the present paper, we have shown that, under UV light activation, Ru(PPh₃)₃Cl₂ exhibits an interesting photocleavage ability to generate phenyl radicals being able to (i) initiate a (meth)acrylate polymerization and (ii) react with THF. This last reaction is particularly important when using a Ru-

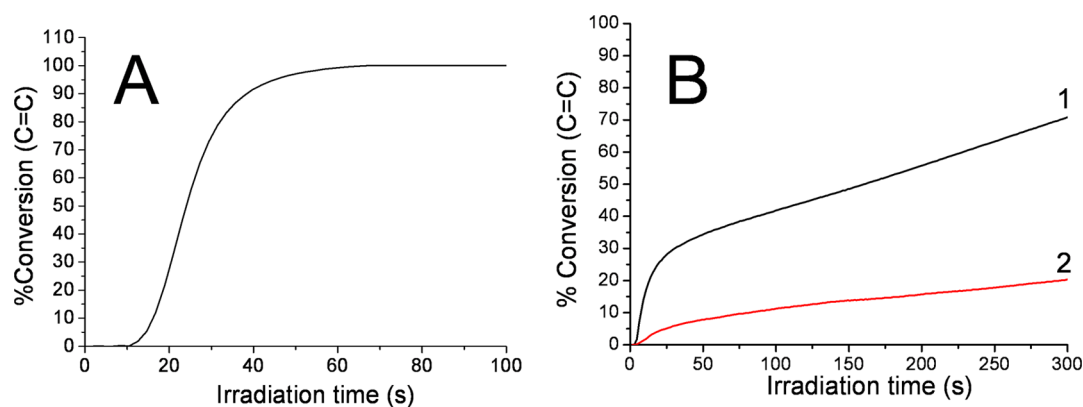


Figure 9. Photopolymerization profiles. A) Poly(ethylene glycol) (400) diacrylate (PEGDA) in the presence of $\text{Ru}(\text{PPh}_3)_3\text{Cl}_2$ (1 wt %). B) Ethoxylated bisphenol A dimethacrylate (EBDMA) in the presence of (1) $\text{Ru}(\text{PPh}_3)_3\text{Cl}_2$ (1 wt %) and (2) absence of $\text{Ru}(\text{PPh}_3)_3\text{Cl}_2$. In laminate. Polychromatic Xe–Hg lamp irradiation; $I_0 = 150 \text{ mW cm}^{-2}$.

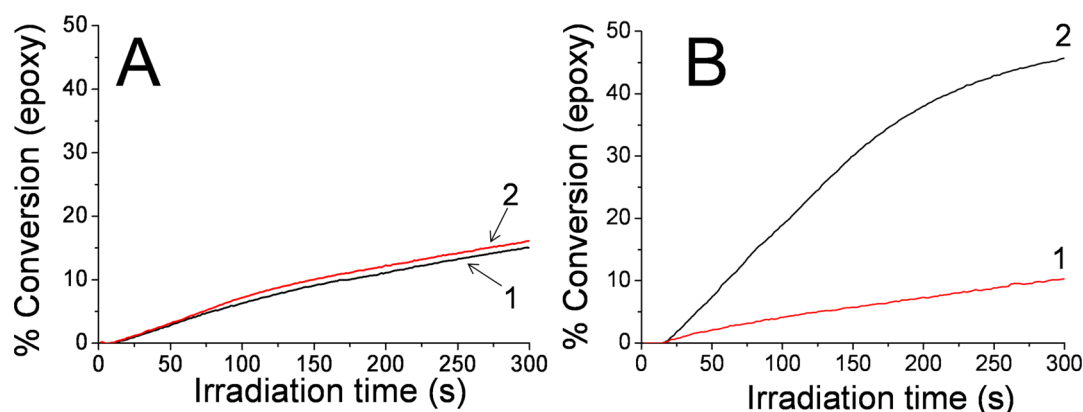


Figure 10. Photopolymerization profiles of a diepoxide in the presence of (A) (1) $\text{Ru}(\text{PPh}_3)_3\text{Cl}_2$ (1 wt %)/ACN (0.5 mL) and (2) $\text{Ru}(\text{PPh}_3)_3\text{Cl}_2$ (1 wt %)/ AgSbF_6 (3 wt %)/ACN (0.5 mL) and (B) (1) $\text{Ru}(\text{PPh}_3)_3\text{Cl}_2$ (1 wt %)/THF (0.5 mL) and (2) $\text{Ru}(\text{PPh}_3)_3\text{Cl}_2$ (1 wt %)/ AgSbF_6 (3 wt %)/THF (0.5 mL). In laminate. Polychromatic Xe–Hg lamp irradiation; $I_0 = 150 \text{ mW cm}^{-2}$.

$(\text{PPh}_3)_3\text{Cl}_2$ /silver salt/THF photoinitiating system as it allows (i) the efficient polymerization of a cationic matrix and (ii) the concomitant *in situ* production of $\text{Ag}(0)$ NPs. This approach evidences the role of the phosphine ligands in the ruthenium complex series toward photopolymerization processes and should broaden the application portfolio of such compounds. It could also be the starting point of further studies for developing biobased antibacterial coatings.

■ ASSOCIATED CONTENT

📄 Supporting Information

^1H and ^{13}C liquid NMR spectra of isosorbide diglycidyl ether in CDCl_3 and molecular orbital transition for the single state of $\text{Ru}(\text{PPh}_3)_3\text{Cl}_2$ at 615 nm computed at the B3LYP/LANL2DZ level. This material is available free of charge via the Internet at <http://pubs.acs.org>.

■ AUTHOR INFORMATION

Corresponding Author

*E-mail: (D.L.V.) versace@icmpe.cnrs.fr; (J.L.) jacques.lalevee@uha.fr.

Notes

The authors declare no competing financial interest.

#Retired.

■ ACKNOWLEDGMENTS

The authors would like to thank the CNRS Institute for financial support.

■ REFERENCES

- (1) Hanyu, A.; Takezawa, E.; Sakaguchi, S.; Ishii, Y. *Tetrahedron Lett.* **1998**, 39 (31), 5557–5560.
- (2) Zhou, Y.-G.; Tang, W.; Wang, W.-B.; Li, W.; Zhang, X. *J. Am. Chem. Soc.* **2002**, 124 (18), 4952–4953.
- (3) Matteoli, U.; Bianchi, M.; Frediani, P.; Menchi, G.; Botteghi, C.; Marchetti, M. *J. Organomet. Chem.* **1984**, 263 (2), 243–246.
- (4) Bergounhou, C.; Fompeyrine, P.; Commenges, G.; Bonnet, J. J. *J. Mol. Catal.* **1988**, 48 (2–3), 285–312.
- (5) (a) de Vries, J. G.; Roelfes, G.; Green, R. *Tetrahedron Lett.* **1998**, 39 (45), 8329–8332. (b) Jenner, G.; Nahmed, E. M.; Leismann, H. *J. Organomet. Chem.* **1990**, 387 (3), 315–321.
- (6) (a) Schwab, P.; Grubbs, R. H.; Ziller, J. W. *J. Am. Chem. Soc.* **1996**, 118 (1), 100–110. (b) Lynn, D. M.; Mohr, B.; Grubbs, R. H. *J. Am. Chem. Soc.* **1998**, 120 (7), 1627–1628.
- (7) (a) Terashima, T.; Ouchi, M.; Ando, T.; Sawamoto, M. *J. Am. Chem. Soc.* **2006**, 128 (34), 11014–11015. (b) Fukuzaki, Y.; Tomita, Y.; Terashima, T.; Ouchi, M.; Sawamoto, M. *Macromolecules* **2010**, 43 (14), 5989–5995. (c) Hamasaki, S.; Kamigaito, M.; Sawamoto, M. *Macromolecules* **2002**, 35 (8), 2934–2940.
- (8) Nishikawa, T.; Ando, T.; Kamigaito, M.; Sawamoto, M. *Macromolecules* **1997**, 30 (8), 2244–2248.
- (9) Shibata, T.; Satoh, K.; Kamigaito, M.; Okamoto, Y. *J. Polym. Sci., Part A: Polym. Chem.* **2006**, 44 (11), 3609–3615.

- (10) Matsumoto, H.; Nakano, T.; Nagai, Y. *Tetrahedron Lett.* **1973**, *14* (51), 5147–5150.
- (11) (a) Kato, M.; Kamigaito, M.; Sawamoto, M.; Higashimura, T. *Macromolecules* **1995**, *28* (5), 1721–1723. (b) Ando, T.; Kato, M.; Kamigaito, M.; Sawamoto, M. *Macromolecules* **1996**, *29* (3), 1070–1072. (c) Ando, T.; Kamigaito, M.; Sawamoto, M. *Macromolecules* **2000**, *33* (18), 6732–6737. (d) Matsuyama, M.; Kamigaito, M.; Sawamoto, M. *J. Polym. Sci., Part A: Polym. Chem.* **1996**, *34* (17), 3585–3589.
- (12) Fouassier, J. P.; Lalevée, J. *Photoinitiators for Polymer Synthesis: Scope, Reactivity, and Efficiency*; Wiley: New York, 2013.
- (13) Cunningham, A. F.; Desobry, V. In *Radiation Curing in Polymer Science and Technology*; Fouassier, J. P., Rabek, J. F., Eds.; Elsevier: Barking, U.K., 1993; Vol. 2, pp 323–374.
- (14) (a) Delaude, L.; Demonceau, A.; Noels, A. F. *Chem. Commun.* **2001**, *11*, 986–987. (b) Wang, D.; Wurst, K.; Knolle, W.; Decker, U.; Prager, L.; Naumov, S.; Buchmeiser, M. R. *Angew. Chem., Int. Ed.* **2008**, *47* (17), 3267–3270. (c) Ben-Asuly, A.; Aharoni, A.; Diesendruck, C. E.; Vidavsky, Y.; Goldberg, I.; Straub, B. F.; Lemcoff, N. G. *Organometallics* **2009**, *28* (16), 4652–4655. (d) Delaude, L.; Szyba, M.; Demonceau, A.; Noels, A. F. *Adv. Synth. Catal.* **2002**, *344* (6–7), 749–756.
- (15) Lalevée, J.; Dumur, F.; Mayer, C. R.; Gigmès, D.; Nasr, G.; Tehfe, M.-A.; Telitel, S.; Morlet-Savary, F.; Graff, B.; Fouassier, J. P. *Macromolecules* **2012**, *45* (10), 4134–4141.
- (16) (a) Zhang, G.; Song, I. Y.; Ahn, K. H.; Park, T.; Choi, W. *Macromolecules* **2011**, *44* (19), 7594–7599. (b) Alfredo, N. V.; Jalapa, N. E.; Morales, S. L.; Ryabov, A. D.; Le Lagadec, R.; Alexandrova, L. *Macromolecules* **2012**, *45* (20), 8135–8146.
- (17) (a) Uygun, M.; Kahveci, M. U.; Odaci, D.; Timur, S.; Yagci, Y. *Macromol. Chem. Phys.* **2009**, *210* (21), 1867–1875. (b) Yagci, Y.; Sangermano, M.; Rizza, G. *Chem. Commun.* **2008**, *24*, 2771–2773. (c) Stampelcoskie, K. G.; Scaiano, J. C. *Photochem. Photobiol.* **2012**, *88* (4), 762–768. (d) Scaiano, J. C.; Stampelcoskie, K. G.; Hallett-Tapley, G. L. *Chem. Commun.* **2012**, *48* (40), 4798–4808. (e) Pacioni, N. L.; Pardoe, A.; McGilvray, K. L.; Chretien, M. N.; Scaiano, J. C. *Photochem. Photobiol. Sci.* **2010**, *9* (6), 766–774. (f) Marin, M. L.; McGilvray, K. L.; Scaiano, J. C. *J. Am. Chem. Soc.* **2008**, *130* (49), 16572–16584. (g) Sangermano, M.; Roppolo, I.; Camara, V. H. A.; Dizman, C.; Ates, S.; Torun, L.; Yagci, Y. *Macromol. Mater. Eng.* **2011**, *296* (9), 820–825. (h) Versace, D.-L.; Ramier, J.; Grande, D.; Andaloussi, S. A.; Dubot, P.; Hobeika, N.; Malval, J.-P.; Lalevée, J.; Renard, E.; Langlois, V. *Adv. Healthcare Mater.* **2013**, *2* (7), 1008–1018. (i) Malval, J.-P.; Jin, M.; Balan, L.; Schneider, R. I.; Versace, D.-L.; Chaumeil, H. I. n.; Defoin, A.; Soppera, O. *J. Phys. Chem. C* **2010**, *114* (23), 10396–10402. (j) Scaiano, J. C.; Aliaga, C.; Maguire, S.; Wang, D. *J. Phys. Chem. B* **2006**, *110* (26), 12856–12859.
- (18) Łukaszczyk, J.; Janicki, B.; Frick, A. *J. Mater. Sci.: Mater. Med.* **2012**, *23* (5), 1149–1155.
- (19) Tehfe, M.-A.; Lalevée, J.; Gigmès, D.; Fouassier, J. P. *Macromolecules* **2010**, *43* (3), 1364–1370.
- (20) Lalevée, J.; Blanchard, N.; Tehfe, M.-A.; Peter, M.; Morlet-Savary, F.; Gigmès, D.; Fouassier, J. P. *Polym. Chem.* **2011**, *2* (9), 1986–1991.
- (21) La Placa, S. J.; Ibers, J. A. *Inorg. Chem.* **1965**, *4* (6), 778–783.
- (22) Martin, R. L. *J. Chem. Phys.* **2003**, *118* (11), 4775–4777.
- (23) Lalevée, J.; Blanchard, N.; Tehfe, M.-A.; Morlet-Savary, F.; Fouassier, J. P. *Macromolecules* **2010**, *43* (24), 10191–10195.
- (24) Sakaguchi, Y.; Hayashi, H. *Chem. Phys. Lett.* **1995**, *245* (6), 591–597.
- (25) (a) Caram, J. A.; Vasini, E. J. *Electrochim. Acta* **1994**, *39* (16), 2395–2400. (b) Ohmori, H.; Nakai, S.; Masui, M. *J. Chem. Soc., Perkin Trans. 1* **1978**, No. 11, 1333–1335. (c) Schiavon, G.; Zecchin, S.; Cogoni, G.; Bontempelli, G. *J. Electroanal. Chem. Interface Electrochem.* **1973**, *48* (3), 425–431.
- (26) Maillard, M.; Huang, P.; Brus, L. *Nano Lett.* **2003**, *3* (11), 1611–1615.
- (27) Dursun, C.; Degirmenci, M.; Yagci, Y.; Jockusch, S.; Turro, N. J. *Polymer* **2003**, *44* (24), 7389–7396.
- (28) Abdul-Rasoul, F. A. M.; Ledwith, A.; Yagci, Y. *Polym. Bull.* **1978**, *1* (1), 1–6.